Earthquakes and Structures, *Vol. 7, No. 6 (2014) 969-999*
DOI: http://dx.doi.org/10.12989/eas.2014.7.6.969

Optimal design of the seismic protection system for isolated bridges

Daniele Losanno*, Mariacristina Spizzuoco[a], Giorgio Serino[b]

Department of Structures for Architecture and Engineering, University Federico II, Via Claudio 21, 80125, Naples, Italy

(Received February 13, 2014, Revised June 1, 2014, Accepted June 10, 2014)

Abstract. Aim of the paper is the definition of optimal design parameters characterizing the isolation system of a bridge, both in the case of elastomeric (VI) and sliding bearings (SI), having viscoelastic or rigid-plastic behavior, respectively, installed between the piers and the deck. The problem is treated by means of an analytical approach. Using the frequency response analysis, a simple procedure is proposed to determine the optimal value of the viscous coefficient or the yield displacement of the isolators. The adequacy of the proposed procedure is finally verified through time-history analyses performed on a practical case under natural earthquakes.

Keywords: seismic response; isolated bridge; optimal design; damping; elastomeric bearings; sliding bearings

1. Introduction

The seismic protection of bridge decks by using passive isolation systems represents a widely studied technique since the Eighties (Bhuiyan and Alam 2013), even though different more complex control strategies (e.g., semi-active and active ones) have been investigated and implemented in civil structures in the last twenty years (Li and Liu 2011; Li, Liu and Lan 2012). The design of a passive isolation system for bridges is often treated as an optimization problem: once the objective of the optimization is defined, together with the constraints imposed by the problem, the design methodology is developed with the aim to determine the optimal mechanical characteristics of the protection devices. In the following, some proposals of different researchers will be summarized, first reporting those adopting optimization concepts in formulating the design criteria.

Ciampi and De Angelis (1996) and Ciampi (1998) proposed an energy-based methodology for the optimal design of dissipation devices used as base isolation systems of typical bridges. The approach consisted in the maximization of an appropriate nondimensional energy index defined as the ratio between the energy dissipated by the isolators and the input energy to the controlled

*Corresponding author, Ph.D. Candidate, E-mail: daniele.losanno@unina.it
[a]Ph.D., E-mail: spizzuoc@unina.it
[b]Professor, E-mail: serino@unina.it

http://www.techno-press.org/?journal=eas&subpage=7 ISSN: 2092-7614 (Print), 2092-7622 (Online)

bridge. Preliminary numerical results on a single degree of freedom (DOF) system allowed to build manageable design graphs of the optimal mechanical characteristics of the dissipative devices. Further curves were also provided for a check of the relevant structural response quantities and the damage level suffered by the devices.

Liu (2002) presented a new phase-plane estimation method of periodic elastoplastic solutions for the steady-state response of the single DOF bilinear elastoplastic oscillator under sinusoidal loadings. Three dimensionless ratios, namely stiffness ratio, force ratio and frequency ratio, as well as an elastic-phase duration variable were identified. The new estimate offered closed-form formulae for the force ratio and the adimensionalized maximum displacement, with respect to the yield displacement, in terms of stiffness ratio, frequency ratio and elastic-phase duration variable. The maximization of the dissipation efficiency is also pursued.

Hwang & Tseng (2005) derived some design formulas for both supplemental linear and non-linear viscous dampers to bridge structures. The damping coefficients of the added dampers were determined based on the concept of "composite damping ratio" in which the bridge components such as rubber bearings, piers and abutments may have different stiffnesses, lumped masses and damping ratios. In addition to the validation on a two DOFs simplified bridge model, a three-span bridge model was also used for the seismic response analysis, showing a good agreement with the proposed design formulas.

Paolacci (2013) proposed a criterion to optimize the characteristics of viscoelastic control devices, based on an energy-based index (EDI) as objective function. An optimal design of the control system was obtained by maximizing the EDI index. An interesting outcome was that the multi-objective nature of the index induced a simultaneous reduction of both kinematic and static response quantities. The optimization procedure was applied to a single DOF system, representative of a structure equipped with viscoelastic dampers (VED): the behavior of the latter was modelled using a Maxwell unit. The comparison of the response to simple excitations, like harmonic and white-noise inputs, with the response to synthetic accelerograms, showed that the optimal design of the VED was practically independent of the input. This means that it is possible to obtain preliminary indications on the optimal characteristics of the dampers, even in closed form.

On the other hand, other authors proposed to single out the optimal control system by the results of a wide parametrical investigation on benchmark bridges.

Madhekar and Jangid (2009) presented the dynamic behavior of benchmark highway bridges using variable dampers under six bidirectional earthquake ground motions: a viscous damper was used as a passive control device and a variable damper, developed from a magnetorheological (MR) damper, was used as a semi-active control device. The study was based on the simplified lumped-mass finite element model of a highway bridge in Southern California. The prime aim of the study was to investigate the effectiveness of viscous dampers and variable dampers with a friction-type damping force scheme and a two-step viscous damping force scheme, with important parametric variation. Numerical simulations were conducted by installing the devices between the deck and abutments of the bridge: the seismic response of the bridge was compared with the corresponding uncontrolled case, and controlled by alternative sample control strategies.

Ozbulut & Hurlebaus (2010) investigated the seismic response of a multi-span continuous bridge isolated with novel superelastic-friction base isolator (S-FBI), under near-field earthquakes. The isolation system consisted of a flat steel-Teflon sliding bearing and a superelastic NiTi shape memory alloy (SMA) device: while the sliding bearing decouples the superstructure of the bridge

from its piers and dissipates energy through friction, the SMA device provides restoring force and additional damping. The key design parameters of an S-FBI system were the natural period of the isolated bridge, the yielding displacement of the SMA device, and the friction coefficient of the sliding bearings. The goal of this study was to obtain optimal values for each design parameter by performing sensitivity analysis of a bridge isolated by an S-FBI system.

In the present paper, the authors adopt the same philosophical approach presented in previous works (Di Marzo *et al*. 2000, Paolacci and Serino 2001), aiming to define the optimal design of an isolation system, in case of elastomeric and sliding bearings. In these two cited works, a simple operative procedure is delivered for singling out the optimal design parameter of a simple 1-DOF system representing an isolated simply supported bridge or a building's isolated floor. The optimal design parameter, in case of both viscoelastic and rigid-plastic isolators, is defined under the action of a harmonic excitation, and then verified for a case study subjected to a seismic input.

The proposed paper presents a more complete design methodology for the isolation system, installed between the piers and the bridge deck. This methodology is the result of a detailed analytical treatment of simple dynamic systems incorporating the viscoelastic or rigid-plastic dissipative behaviors. With respect to the authors' previous works, the optimization process is developed also in terms of top pier displacements, besides the deck displacements. Moreover, the proposed procedure include specific seismic numerical analyses able to immediately confirm the analytical results or, eventually, state the need of a further iteration.

The design procedure proposed in the present paper is based on a different approach with respect to those adopted by other authors, developing different optimization concepts in formulating the design criteria. In Ciampi and De Angelis (1996), Ciampi (1998) and Paolacci (2013), an energy-based index, related to the energy dissipated by the devices, is formulated as objective function to maximize. Hwang & Tseng (2005) provided design formulas for supplemental linear and non-linear viscous devices for bridge structures, as a function of the desired dissipation level, assumed as given and not correlated to response parameters of the structure. Yang *et al.* (2002) defined two optimal design methodologies for passive energy dissipating devices based on active control theories, including H_∞ and H_2 performances, respectively, capable of determining the optimal locations and the corresponding capacities of the devices.

2. Steady-state response of an isolated bridge subjected to a harmonic base motion

The behavior of a simply supported bridge isolated by means of viscoelastic (i.e. laminated rubber bearing *LRB*) or rigid-plastic devices (i.e. friction pendulum system *FPS*), is analyzed (Fig. 1 (a)).

The dynamic model simulating such a simple structure is also illustrated in the same figure: it is a 2 DOFs model (x, x_c), where the parameters k_c and k_i are the total lateral stiffness of the columns and the bearings, respectively. The procedure is valid in the case of i columns having the same stiffness k_{c1}, being $k_c = i \cdot k_{c1}$, and j isolators of equal stiffness k_{i1}, being $k_i = j \cdot k_{i1}$. The damping behavior is completely defined by the damping coefficient c (in the case of viscoelastic isolators – *VI*) or by the yield strength F_y (in the case of rigid-plastic or sliding isolators – *SI*) of the whole isolation system, thus neglecting damping in the columns. Moreover, m and m_c are the mass of the

deck and the participating mass of all piers, respectively. It is worth to note that, in most cases, m_c is small compared to m and therefore can be neglected, so that the model reduces to a single dynamic DOF with two kinematic DOFs (Fig. 1 (b)).

The dynamic problem of the bridge subjected to a harmonic base excitation can be formulated and solved as shown in the following. The equations of motion are derived together with the definition of the relevant design parameters and response quantities, and the optimal damping characteristics are obtained under the hypothesis that the ratio $k = k_c / k_i$ and the deck mass m are known. For both *VI* and *SI* cases, a closed-form solution of the response is obtained.

Even if earthquake motion is usually random, by means of the Discrete Fourier Trasform Function (DFT), properly working on non-periodic data, it can be decomposed into a linear combination of harmonic functions. Typical ground motions contain a wide range of frequencies and system displacement response shows a dominant period very close to the its natural period. A sweeping frequency of the excitation (i.e., harmonic function with $0 \le \omega \le \infty$) at the base is assumed, since due to extremely different values of the damping parameter, the effective frequency of the system vary significantly. In addition to this, for a damped system, the higher is the damping the shorter will be the transitory condition so that structural response will tend to a single period harmonic function.

The problem is first solved by making reference to the deck displacement x: the optimization procedure is developed with the aim to determine the value of the normalized device's damping parameter ($\nu_{i,opt}$ or δ_{opt}) corresponding to the minimum deck displacement over the whole range of frequency excitation.

On the other hand, different parameters can be also assumed as reference: the displacement of columns x_c in order to control the column base shear, or the relative displacement $x - x_c$ in the isolators in order to check the maximum allowable movement between the deck and the top of columns.

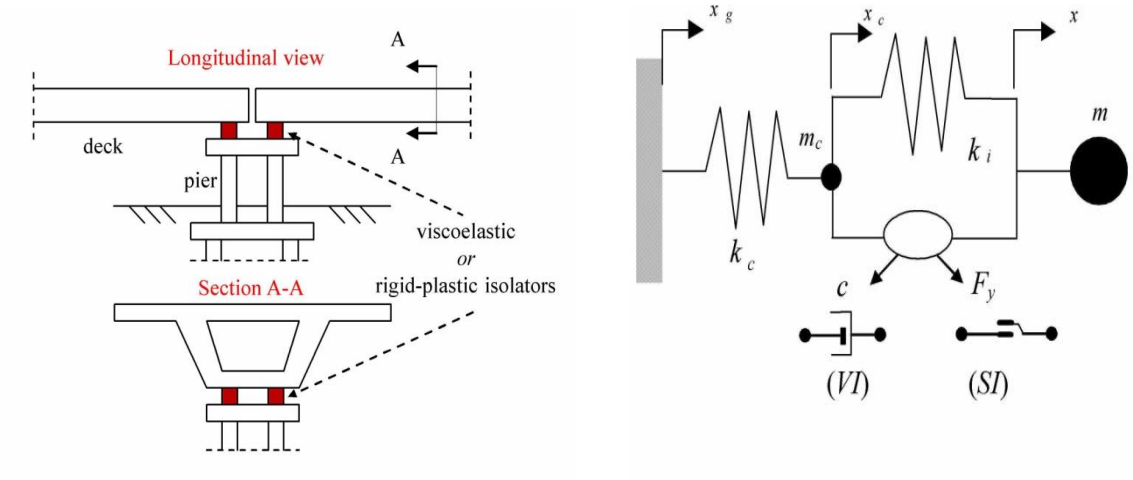

(a) (b)

Fig. 1 (a) Bridge structure and (b) rheological model

2.1 Formulation of the equation of motion

Neglecting the participating mass of the piers (m_c = 0), the general expression of the equation of motion for the model illustrated in Fig.1 (b), subjected to a harmonic base displacement $x_g(t) = x_{g,\max} \cdot \cos \overline{\omega} t$, is simply the following:

$$m\ddot{x} + F(x, x_c, \dot{x}, \dot{x}_c, ...) = m\overline{\omega}^2 x_{g,\max} \cos \overline{\omega} t \tag{1}$$

where x is the relative deck displacement, $F(x, x_c, \dot{x}, \dot{x}_c, ...)$ is the linear or non-linear restoring force in the whole system and dot notation represents derivation with respect to time.

In order to single out the relevant design parameters of the control devices and the structural response parameters, it is needed to write Eq. (1) in an adimensionalized form. Afterwards, introducing the non-dimensional time $\tau = \Omega t$, a different normalized form of the equation of motion can be found, being Ω a normalization frequency corresponding to the natural frequency of the system in one of the three following cases:

i) infinitely stiff piers ($k_c \to \infty$): $\omega_i = \sqrt{k_i / m}$

ii) undamped system ($c = 0$ or $F_y = 0$): $\omega_b = \sqrt{k_c k_i / (k_c + k_b) \cdot m}$

iii) not isolated bridge ($k_i \to \infty$): $\omega_c = \sqrt{k_c / m}$

Considering the non-dimensional time parameter $\tau = \omega_i \, t$, Eq. (1) can be expressed as:

$$\omega_i^2 x''(\tau) + \frac{F(x, x_c, \dot{x}, \dot{x}_c, ...)}{m} = \overline{\omega}^2 x_{g,\max} \cos \beta \tau \tag{2}$$

where ($'$) represents derivation with respect to τ . After simple manipulations:

$$x''(\tau) + \frac{F(x, x_c, \dot{x}, \dot{x}_c, ...)}{m\omega_i^2} = \beta^2 x_{g,\max} \cos \beta \tau \tag{3}$$

$$\zeta''(\tau) + \frac{F(x, x_c, \dot{x}, \dot{x}_c, ...)}{m\omega_i^2 x_{g,\max}} = \beta^2 \zeta(\tau) \cos \beta \tau \tag{4}$$

$$\zeta''(\tau) + \kappa f(\zeta) = \beta^2 \zeta(\tau) \cos \beta \tau \tag{5}$$

where $\zeta = x / x_{g,\max}$ is the normalized deck displacement, $f(\zeta) = F(x, x_c, \dot{x}, \dot{x}_c, ...) / k_c x_{g,\max}$ is the normalized restoring force, $\beta = \overline{\omega} / \omega_i$ is the normalized frequency. Eq. (5) represents the final form of the normalized equation of motion and it is developed in the following paragraphs for the two defined cases.

2.2 Solution of the equation of motion for the VI case

In the case of viscoelastic isolators (*VI*) having damping coefficient c , the equivalent damping ratio is defined as:

$$\nu_i = \frac{c}{2m\omega_i} \tag{6}$$

The force in the passive control system, i.e. the base shear of the pier, can be expressed in the frequency domain trough the complex response method:

$$F(\overline{\omega}) = (k_i + i\overline{\omega}c) \cdot (x(\overline{\omega}) - x_c(\overline{\omega})) \tag{7}$$

Since the top column displacement is given by $x_c(\overline{\omega}) = F(\overline{\omega})/k_c$, Eq. (7) can be rewritten as:

$$F(\overline{\omega}) = (k_i + i\overline{\omega}c) \cdot (x(\overline{\omega}) - \frac{F(\overline{\omega})}{k_c}) = K_d(\overline{\omega}) \cdot x(\overline{\omega}) \tag{8}$$

where:

$$K_d(\overline{\omega}) = \frac{F(\overline{\omega})}{x(\overline{\omega})} = \frac{k_i + i\overline{\omega}c}{1 + \dfrac{k_i + i\overline{\omega}c}{k_c}} \tag{9}$$

represents the complex stiffness of the controlled bridge.

Dividing Eq. (9) by k_c, the dimensionless system stiffness is:

$$\overline{K}_d(\overline{\omega}) = \frac{\dfrac{1}{\kappa} + \dfrac{i\overline{\omega}c}{k_c}}{\dfrac{1+\kappa}{\kappa} + \dfrac{i\overline{\omega}c}{k_c}} \tag{10}$$

Substituting Eq. (6) in Eq. (10), the normalized stiffness becomes:

$$\overline{K}_d(\beta) = \frac{\dfrac{1}{\kappa} + \dfrac{i2\nu_i\beta}{\kappa}}{\dfrac{1+\kappa}{\kappa} - \dfrac{i2\nu_i\beta}{\kappa}} = \frac{\dfrac{(1+\kappa)}{\kappa^2} + 4\nu_i{}^2\dfrac{\beta^2}{\kappa^2}}{(\dfrac{1+\kappa}{\kappa})^2 + 4\nu_i{}^2\dfrac{\beta^2}{\kappa^2}} + i\frac{2\nu_i\dfrac{\beta}{\kappa}}{(\dfrac{1+\kappa}{\kappa})^2 + 4\nu_i{}^2\dfrac{\beta^2}{\kappa^2}} = \tag{11}$$

$$= \overline{K}'_d(\beta) + i\overline{K}''_d(\beta)$$

where $\overline{K}'_d(\beta)$ and $\overline{K}''_d(\beta)$ are, respectively, the overall normalized storage and loss modulus of the controlled bridge.

The normalized restoring force of Eq. (5) thus specifies as:

$$f(\zeta) = \overline{K}_d(\beta) \cdot \zeta \tag{12}$$

and is illustrated in Fig. 2.

The global dynamic behavior of a rubber isolated bridge is completely defined by three parameters: κ, ν_i and β.

In this case, the system is linear and an exact solution for the steady-state response can be evaluated. The solution of Eq. (5) is extremely straightforward using the frequency domain approach.

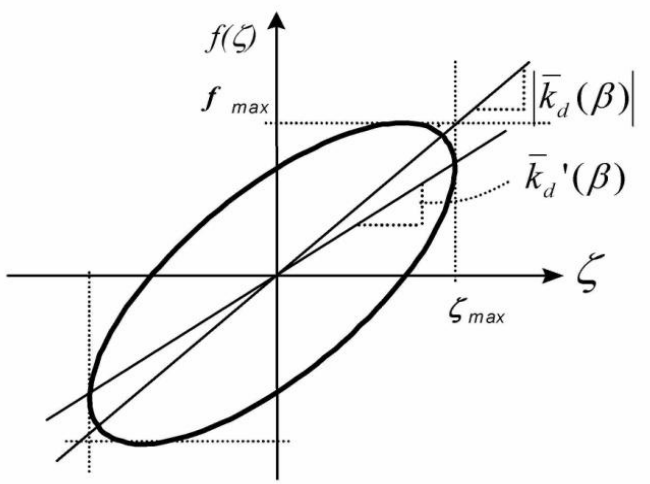

Fig. 2 Normalized restoring force - displacement relationship for the *VI* case

Assuming that a solution of Eq. (5) can be expressed in the form $\zeta(\tau) = \zeta_{\max}(\beta)e^{i(\beta\tau+\phi(\tau))}$, the Fourier transform applied to Eq. (5) gets:

$$-\beta^2\zeta_{\max}(\beta) + \kappa(\bar{K}_d'(\beta) + i\bar{K}_d''(\beta))\zeta_{\max}(\beta) = \beta^2 \tag{13}$$

where the storage modulus $\bar{K}_d'(\beta)$ and loss modulus $\bar{K}_d''(\beta)$ are those defined in Eq. (11). From Eq. (13) it is possible to express the complex response of the bridge in terms of maximum deck displacement:

$$\zeta_{\max}(\beta) = \frac{\beta^2}{\left[\kappa\bar{K}_d'(\beta) - \beta^2\right] + i\kappa\bar{K}_d''(\beta)} \tag{14}$$

The amplitude of the response and its phase angle can be evaluated respectively as the modulus and the argument of the above complex relationship:

$$|\zeta_{\max}(\beta)| = \frac{\beta^2}{\sqrt{\left[\kappa\bar{K}_d'(\beta) - \beta^2\right]^2 + \kappa^2\bar{K}_d''(\beta)^2}} \tag{15}$$

$$\tan\phi(\beta) = \frac{\kappa\bar{K}_d''(\beta)}{\kappa\bar{K}_d'(\beta) - \beta^2} \tag{16}$$

The relations (15) and (16) are simply an extension of the classical amplitude – frequency and phase angle – frequency relationships for a standard linear elastic oscillator subjected to a harmonic base motion.

Introducing the definitions of storage and loss moduli in (15) and (16), they become:

$$|\zeta_{\max}(\beta)| = \frac{\beta^2}{\sqrt{\left[\frac{\frac{(1+\kappa)}{\kappa} + 4\nu_i{}^2\frac{\beta^2}{\kappa}}{\left(\frac{1+\kappa}{\kappa}\right)^2 + 4\nu_i{}^2\frac{\beta^2}{\kappa^2}} - \beta^2\right]^2 + \kappa^2\left(\frac{2\nu_i\frac{\beta}{\kappa}}{\left(\frac{1+\kappa}{\kappa}\right)^2 + 4\nu_i{}^2\frac{\beta^2}{\kappa^2}}\right)^2}} \tag{17}$$

$$\tan\phi(\beta) = \frac{2\nu_i\beta}{\frac{(1+\kappa)}{\kappa} + 4\nu_i{}^2\frac{\beta^2}{\kappa} - \beta^2} \tag{18}$$

Eq. (17) is plotted in Fig. 3 for different values of κ and damping ratio ν_i.

The two limit cases, for which the behavior reduces to an elastic undamped system, are the following:

- $\nu_i = 0 \quad \Rightarrow \quad c = 0$ (no damping)

$$|\zeta_{\max}(\beta)| = \frac{\beta^2}{\frac{\kappa}{1+\kappa} - \beta^2} \tag{19}$$

$$\beta_{resonance} = \sqrt{\frac{\kappa}{(1+\kappa)}}$$

- $\nu_i \to +\infty \quad \Rightarrow \quad c \to +\infty$ (infinite damping)

$$|\zeta_{\max}(\beta)| = \frac{\beta^2}{\kappa - \beta^2} \tag{20}$$

$$\beta_{resonance} = \sqrt{\kappa}$$

The two limit curves intersect in the point of coordinates $\overline{\beta} = \sqrt{\left(2\kappa + \kappa^2\right)/\left[2(1+\kappa)\right]}$ and $\zeta_{\max}\left(\overline{\beta}\right) = (2+\kappa)/\kappa$. A very low value of ν_i produces a peak of the curve near to the one of the no damping limit case. This peak decreases as far as ν_i increases but a large increase of the damping coefficient induces a shift of the resonance frequency toward the infinite damping limit case, with an increment, at the same time, of the peak amplitude. For $\beta = \overline{\beta}$, Eq. 17 gives $\zeta_{\max}\left(\overline{\beta}\right) = (2+\kappa)/\kappa$ for any other value of ν_i, thus demonstrating that the point of coordinates $(\overline{\beta}, \zeta_{\max}(\overline{\beta}))$ is a common point for all curves.

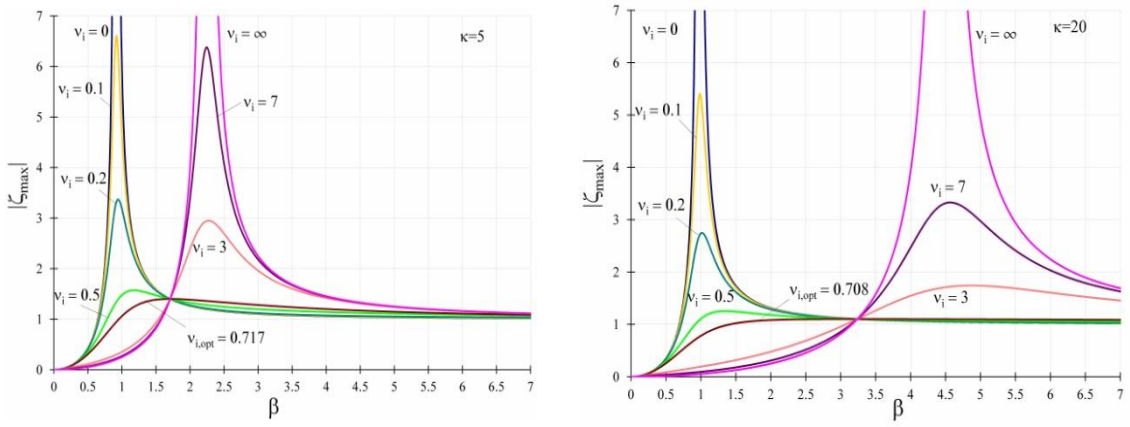

Fig. 3 Maximum deck displacement versus frequency ratio β (κ = 5, 20)

The value of $\nu_{i,opt}$ can be computed by imposing the condition that the above common point ($\overline{\beta}, \zeta_{\max}(\overline{\beta})$) corresponds to the maximum of the generic curve, i.e., by imposing that $\zeta'_{\max}(\overline{\beta}) = 0$. In this way, we get the following 3rd degree equation in the unknown ν_i^2:

$$8(2k+k^2)^3 \upsilon_i^6 + 4(2k^2+3k+1)(2k+k^2)^2(1+k)\upsilon_i^4 + ...$$
$$....+ 2(2k+k^2)(1+k)^5(k-1)\upsilon_i^2 - (1+k)^8 = 0 \tag{21}$$

whose only real solution (all the other solutions are complex) is:

$$\nu_{i,opt} = \sqrt{\frac{(1+\kappa)^2}{2\kappa(2+\kappa)}} \tag{22}$$

Therefore, the minimum resonance peak within the range $\nu_i = [0, +\infty]$ corresponds to the optimal resonance frequency $\beta_{opt} = \overline{\beta}$.

The complex expression of the maximum force in the pier (equal to its normalized displacement), as well as in the control system, is given by:

$$f_c(\beta) = \zeta_{c,\max}(\beta) = \overline{K}_d(\beta) \frac{\beta^2}{\left[\kappa \overline{K}'_d(\beta) - \beta^2\right] + i\kappa \overline{K}''_d(\beta)} \tag{23}$$

Fig. 4 shows the modulus of expression (23) as function of the frequency ratio β. It can be noted again that all curves have a common point corresponding to the intersection between the limit curves. The intersection point has now coordinates $\overline{\beta}_c = \sqrt{\frac{2\kappa}{2+\kappa}}$ and $\overline{\zeta}_{c,\max} = \frac{2}{\kappa}$ but this point does not represent a maximum for all the curves. For $\nu_i \to \infty$ the column displacement is

practically the same as the deck displacement. For all finite values of $\nu_i \neq 0$, $\zeta_{c,\max}(\beta)$ is always lower than $\zeta_{\max}(\beta)$ even if for $\beta \to \infty$ both $\zeta_{\max}(\beta)$ and $\zeta_{c,\max}(\beta)$ tend to 1.

On the other hand, the quantity $\Delta\zeta = \zeta_{\max} - \zeta_{c,\max}$ (see Fig. 5) is always decreasing with increasing ν_i.

An optimization criterion for the design of the control system is the minimization of the maximum displacement $\zeta_{\max}(\beta)$ in the whole range of β, and the check a posteriori of the response in terms of base-shear. This means to select as design parameter the value $\nu_{i,opt}$ given in Eq. 22: a design spectrum is showed in Fig. 6 (a), for several values of κ. High values of damping ratio are required for small values of κ, whereas, for $\kappa > 10$ $\nu_{i,opt}$ remains practically constant around the value 0.7. It is interesting to note in Fig. 6 (b) that the optimum deck displacement, i.e. the minimum resonance peak for any value of κ given by $\nu_{i,opt}$, decreases with κ and tends to 1. For values of κ greater than $20 \div 30$, a small decrease in the optimum response is produced.

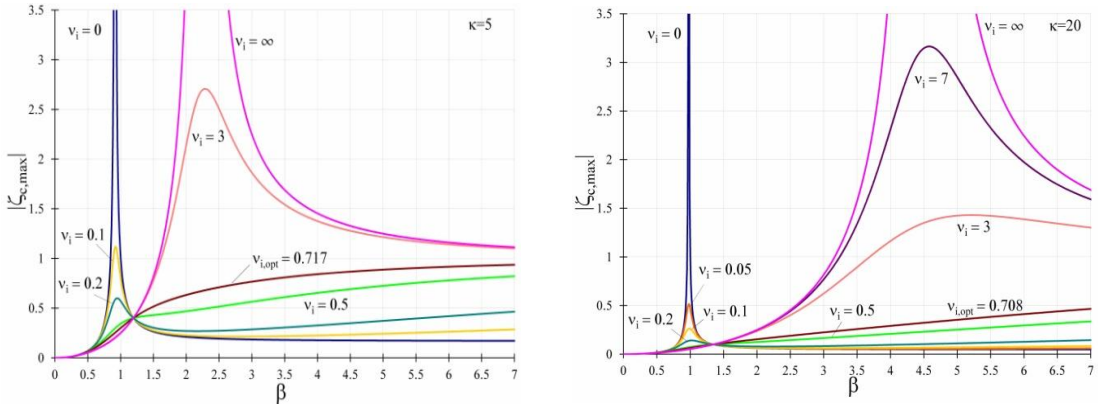

Fig. 4 Top column displacement versus frequency ratio β (κ = 5, 20)

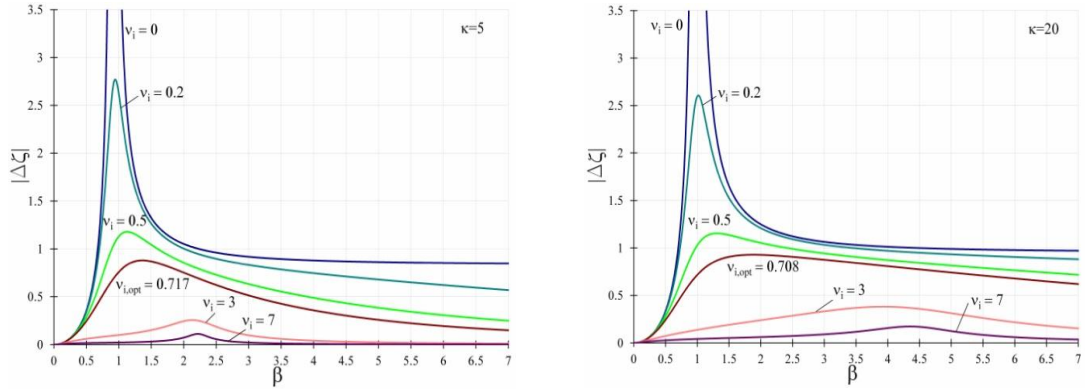

Fig. 5 Relative deck to pier displacement versus frequency ratio β (κ = 5, 20)

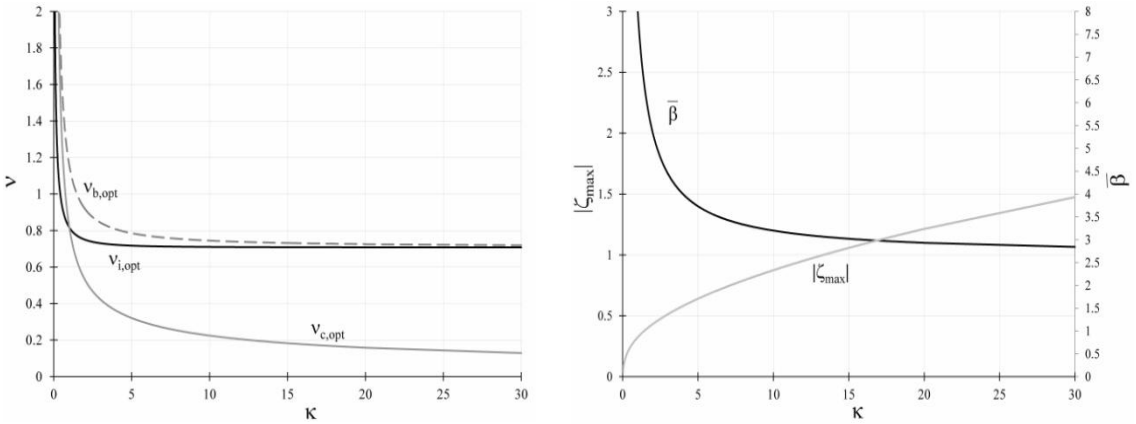

(a) (b)

Fig. 6 (a) *VI* optimal parameters for different normalizations and (b) deck optimal displacement and corresponding frequency ratio versus κ

If the other two expressions of the normalized frequency Ω are used, the expression of the optimal parameter can be easily evaluated as follows, and is also shown in Fig. 6 (a):

$$\nu_{b,opt} = \frac{c_{opt}}{2m\omega_b} = \sqrt{\frac{1+\kappa}{\kappa}}\frac{c_{opt}}{2m\omega_i} = \sqrt{\frac{(1+\kappa)^3}{2\kappa^2(2+\kappa)}} \tag{24}$$

$$\nu_{c,opt} = \frac{c_{opt}}{2m\omega_c} = \frac{1}{\sqrt{\kappa}}\frac{c_{opt}}{2m\omega_i} = \sqrt{\frac{(1+\kappa)^2}{2\kappa^2(2+\kappa)}} \tag{25}$$

2.3 Solution of the equation of motion for the SI case

In the case of sliding isolators (*SI*), the restoring force $F(x, x_c, \dot{x}, \dot{x}_c ...)$ is a bilinear relationship characterized by an initial stiffness k_c and a post-yielding stiffness $k_c k_i / (k_c + k_i)$. The supplemental device has a rigid-plastic behavior (Fig. 7 (a)) modeled by a spring (k_i) acting in parallel with a friction element (sliding force F_y).

The normalized restoring force is shown in Fig. 7 (b). It depends on two dimensionless parameters $\kappa = k_c / k_i$ and δ . The normalized initial stiffness is equal to unity while the post-elastic stiffness becomes $1/(1+\kappa)$; δ is the normalized deck displacement $x_y / x_{g,\max}$ corresponding to the achievement of yielding in the device, and it is equal to the normalized yield strength f_y .

On the basis of the observations above, it is possible to state that the dynamic behavior of the *SI* bridge case is completely defined by the following three dimensionless parameters: κ , δ and β .

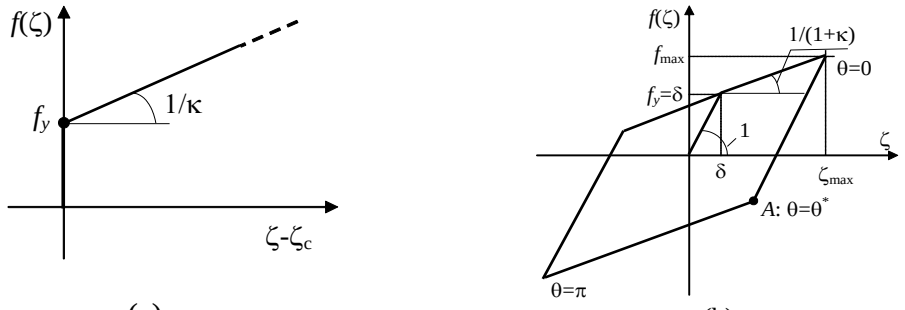

Fig. 7 Normalized restoring force-displacement relationships (a) in the sliding isolators and (b) in the controlled bridge

The equation of motion is non-linear and a closed form solution cannot be easily derived. In the following, the slowly varying parameters method (Caughey 1960) is adopted. It can be reasonably assumed that, under a harmonic base motion, the steady-state response is periodic with frequency β:

$$\zeta(\tau) = \zeta_{\max}(\tau)\cos[\beta\tau + \phi(\tau)] = \zeta_{\max}\cos\theta \tag{26}$$

where $\zeta_{\max}$ and ϕ are slowly varying functions of τ, and $\theta = \beta\tau + \phi(\tau)$. Differentiating Eq. (26) with respect to τ, one obtains:

$$\zeta'(\tau) = -\beta\zeta_{\max}\sin\theta - \zeta_{\max}\phi'\sin\theta + \zeta'_{\max}\cos\theta \tag{27}$$

For the hypotheses of the slowly varying parameters method, it is possible to approximate the values of $\zeta_{\max}$ and ϕ by their mean values and to assume that the velocity $\zeta'(\tau)$ is harmonic, i.e:

$$\zeta'_{\max}\cos\theta - \zeta_{\max}\phi'\sin\theta = 0 \tag{28}$$

Differentiating again Eq. (27) with respect to τ:

$$\zeta''(\tau) = -\beta^2\zeta_{\max}\cos\theta - \beta\zeta_{\max}\phi'\cos\theta - \beta\zeta'_{\max}\sin\theta \tag{29}$$

and substituting it in Eq. (5), leads to:

$$-\beta^2\zeta_{\max}\cos\theta - \beta\zeta_{\max}\phi'\cos\theta - \beta\zeta'_{\max}\sin\theta + \kappa f(\zeta) = \beta^2\zeta_{\max}\cos(\theta - \phi) \tag{30}$$

We can multiply Eq. (30) by $\sin\theta$ and Eq. (28) by $\beta\cos\theta$ and subtract them, thus obtaining:

$$-\beta^2\zeta_{\max}\sin\theta\cos\theta - \beta\zeta'_{\max}\left(\sin^2\theta + \cos^2\theta\right) + \kappa f(\zeta)\sin\theta = \beta^2\cos(\theta - \phi)\sin\theta \tag{31}$$

The average made over one cycle of θ leads to:

$$-\beta\zeta'_{\max} + \frac{1}{2\pi}\int_0^{2\pi}\kappa f(\zeta)\sin\theta d\theta = \frac{\beta^2}{2}\sin\phi \tag{32}$$

Now, multiplying Eq. (28) by $\beta\sin\theta$, Eq. (30) by $\cos\theta$ and adding them:

$$-\beta^2\zeta_{\max}\cos^2\theta-\beta\zeta_{\max}\phi'+\kappa f(\zeta)\cos\theta=\beta^2\cos(\theta-\phi)\cos\theta \tag{33}$$

and averaging over one cycle of θ, one obtains:

$$-\beta\zeta_{\max}\phi'-\frac{\beta^2}{2}\zeta_{\max}+\frac{1}{2\pi}\int_0^{2\pi}\kappa f(\zeta)\cos\theta d\theta=\frac{\beta^2}{2}\cos\phi \tag{34}$$

If $S(\zeta_{\max})$ and $C(\zeta_{\max})$ are the two quantities:

$$\begin{aligned} S(\zeta_{\max})&=\frac{1}{\pi}\int_0^{2\pi}f(\zeta)\sin\theta d\theta \\ C(\zeta_{\max})&=\frac{1}{\pi}\int_0^{2\pi}f(\zeta)\cos\theta d\theta \end{aligned} \tag{35}$$

hence Eqs. (32) and (34) become:

$$\begin{aligned} -2\beta\zeta'_{\max}+\kappa S(\zeta_{\max})&=\beta^2\sin\phi \\ -2\beta\zeta_{\max}\phi'-\beta^2\zeta_{\max}+\kappa C(\zeta_{\max})&=\beta^2\cos\phi \end{aligned} \tag{36}$$

Using Fig. 7 (b), if $\theta^*=\cos^{-1}\left(1-\frac{2\delta}{\zeta_{\max}}\right)$ the quantities $S(\zeta_{\max})$ and $C(\zeta_{\max})$ are readily evaluated:

$$\begin{cases} S(\zeta_{\max})=-\dfrac{\kappa}{1+\kappa}\dfrac{\zeta_{\max}}{\pi}\sin^2\theta^* & \text{if} \quad \zeta_{\max}>\delta \\ S(\zeta_{\max})=0 & \text{if} \quad \zeta_{\max}\le\delta \end{cases} \tag{37}$$

$$\begin{cases} C(\zeta_{\max})=\dfrac{\zeta_{\max}}{\pi}\left[\dfrac{\kappa}{1+\kappa}\theta^*+\dfrac{\pi}{1+\kappa}-\dfrac{\kappa}{2(1+\kappa)}\sin 2\theta^*\right] & \text{if} \quad \zeta_{\max}>\delta \\ C(\zeta_{\max})=\zeta_{\max} & \text{if} \quad \zeta_{\max}\le\delta \end{cases} \tag{38}$$

The steady state response is obtained by setting $\zeta'_{\max}(\tau)$ and $\phi'(\tau)$ equal to zero in Eq. (36), which becomes:

$$\begin{aligned} \kappa S(\zeta_{\max})&=\beta^2\sin\phi \\ \kappa C(\zeta_{\max})-\beta^2\zeta_{\max}&=\beta^2\cos\phi \end{aligned} \tag{39}$$

Eliminating ϕ and β^2 from Eq. (39), we get the following displacement – frequency and phase angle – frequency relationships in the unknowns $\zeta_{\max}$ and ϕ:

$$\left[C(\zeta_{\max})-\frac{\beta^2}{\kappa}\zeta_{\max}\right]^2+\left[S(\zeta_{\max})\right]^2=\frac{\beta^4}{\kappa^2} \tag{40}$$

$$\tan\phi = \frac{S(\zeta_{\max})}{C(\zeta_{\max}) - \dfrac{\beta^2}{\kappa}\zeta_{\max}} \tag{41}$$

Differently from the *VI* case, now it is convenient to express the quantity $\zeta_{\max}$ implicitly as a function of β from Eq. (40):

$$\frac{\beta^2}{\kappa} = \left[\zeta_{\max} C(\zeta_{\max}) \pm \sqrt{\zeta_{\max}^2 C^2(\zeta_{\max}) - \left(\zeta_{\max}^2 - 1\right)\left(C^2(\zeta_{\max}) + S^2(\zeta_{\max})\right)}\right] \Big/ \left(\zeta_{\max}^2 - 1\right) \tag{42}$$

The maximum deck displacement $\zeta_{\max}$ is attained at the point where β^2 has a double root, i.e. for the value $\tilde{\zeta}_{\max}$ which makes void the radical quantity in Eq. (42), i.e. satisfies the equation:

$$\begin{aligned} &\tilde{\zeta}_{\max}^2 = C^2\left(\tilde{\zeta}_{\max}\right) \Big/ S^2\left(\tilde{\zeta}_{\max}\right) + 1 \\ &\tilde{\zeta}_{\max}^2 - \frac{\left\{\kappa \arccos\left(1 - \dfrac{2\delta}{\tilde{\zeta}_{\max}}\right) + \pi - \dfrac{\kappa}{2} sen\left[2\arccos\left(1 - \dfrac{2\delta}{\tilde{\zeta}_{\max}}\right)\right]\right\}^2}{\kappa^2 sen^4\left[\arccos\left(1 - \dfrac{2\delta}{\tilde{\zeta}_{\max}}\right)\right]} - 1 = 0 \end{aligned} \tag{43}$$

and the corresponding frequency is:

$$\tilde{\beta} = \sqrt{\kappa S(\tilde{\zeta}_{\max}) \sqrt{S^2\left(\tilde{\zeta}_{\max}\right) + C^2(\tilde{\zeta}_{\max})} \Big/ C(\tilde{\zeta}_{\max})} \tag{44}$$

The limit cases ($\delta = 0$ and $\delta \to +\infty$) again correspond, respectively, to the case of two springs (k_c and k_i) connected in series or a single spring (k_c), and are expressed as $\beta(\zeta_{\max})$:

- $\delta = 0 \quad \Rightarrow \quad F_{dy} = 0$

$$\beta^2 = \frac{\kappa \zeta_{\max}}{(1+\kappa)(1+\zeta_{\max})} \tag{45}$$

- $\delta \to +\infty \quad \Rightarrow \quad F_{dy} \to +\infty$

$$\beta^2 = \frac{k \zeta_{\max}}{(1+\zeta_{\max})} \tag{46}$$

$$\beta_{resonance} = \sqrt{\kappa}$$

The function $\beta^2(\zeta_{\max})$ in Eq. (42) is a continuous function whose derivative is discontinuous when $\zeta_{\max} = \delta$. This is because the response is linear for any value of $\zeta_{\max} < \delta$, being the flexibility of the system due to the only spring k_c.

By analyzing the frequency response function $\zeta_{\max}(\beta)$, it is possible to figure out the role of

the parameter δ and propose a design methodology for determining its optimal value.

The quantity $\zeta_{\max}$ as a function of β is plotted in Fig. 8 for $\kappa = 5, 20$ and for several values of δ. The point of coordinates $\overline{\beta} = \sqrt{\left(2\kappa + \kappa^2\right) / \left[2\left(1+\kappa\right)\right]}$ and $\zeta_{\max}\left(\overline{\beta}\right) = (2+\kappa)/\kappa$ still represents the intersection of the two limit cases (Eqs. (45) and (46)) but does not belong to all other curves. One notes that a very low value of δ produces a peak of the curve near to the one relative to $\delta = 0$, and its value decreases as far as the previous parameter increases; however, a further increase of the yield displacement induces a shift of the resonance frequency toward the value $\beta = \sqrt{\kappa}$ with an increment of the peak amplitude. Therefore, the resonance peak within the range $\delta = [0, +\infty]$ has a minimum value in correspondence of the frequency β_{opt}, quite close to the one ($\overline{\beta}$) of the intersection point between the limit curves. Therefore, settled a certain κ, the value δ_{opt} is defined as the one which satisfies the condition that its corresponding curve $\zeta_{\max}(\beta)$ has the minimum resonance peak.

In order to get the derived response quantities, simple expressions, involving the normalized displacement $\zeta_{\max}$ and stiffness κ, are introduced. When $\zeta_{\max} > \delta$, the top column displacement $\zeta_{c,\max}$ (equal to the base shear) and the relative displacement $\Delta\zeta = \zeta - \zeta_{c,\max}$ assume the expressions (Fig. 9 and Fig. 10):

$$\zeta_{c,\max} = \frac{\kappa\delta + \zeta_{\max}}{1+\kappa} \tag{47}$$

$$\Delta\zeta = \frac{\kappa(\zeta_{\max} - \delta)}{1+\kappa} \tag{48}$$

while, $\zeta_{c,\max} = \zeta_{\max}$ and $\Delta\zeta = 0$ when $\zeta_{\max} < \delta$.

One notes that once the device yields, the top column displacement $\zeta_{c,\max}$ is always lower than $\zeta_{\max}$ and that the relative displacement $\Delta\zeta$ is always decreasing for increasing values of δ. In addition to this, $\zeta_{c,\max}$ has a maximum value after the yielding of the control device, which is approximately equal to δ for high values of κ, because of the limited force transmitted by the isolator after yielding. This behavior indicates a great advantage of the *SI* system with respect to the *VI* case: rigid-plastic devices apply a strong control on the maximum base-shear force, practically a known value ($\cong F_y$) for high values of κ. Differently from the *VI* case, it is now possible to derive a different optimal value $\delta_{c,opt}$ giving the minimum resonance peak $\zeta_{c,\max}$ in the columns.

A design spectrum has been numerically derived and is plotted in Fig. 11 (a), where both the optimal values δ_{opt} and $\delta_{c,opt}$ are shown as a function of the relative stiffness κ. In Fig. 11 (b) are also plotted both the quantity $\zeta_{\max}(\delta_{opt})$ and $\zeta_{c,\max}(\delta_{c,opt})$, and also the values β_{opt} and $\overline{\beta}$, all versus κ.

From Fig. 11 it is clear that, as far as κ increases, both the optimal parameters and the maximum displacements decrease. Besides, the value of β_{opt} is close to $\overline{\beta}$ and both parameters show a growing trend with κ.

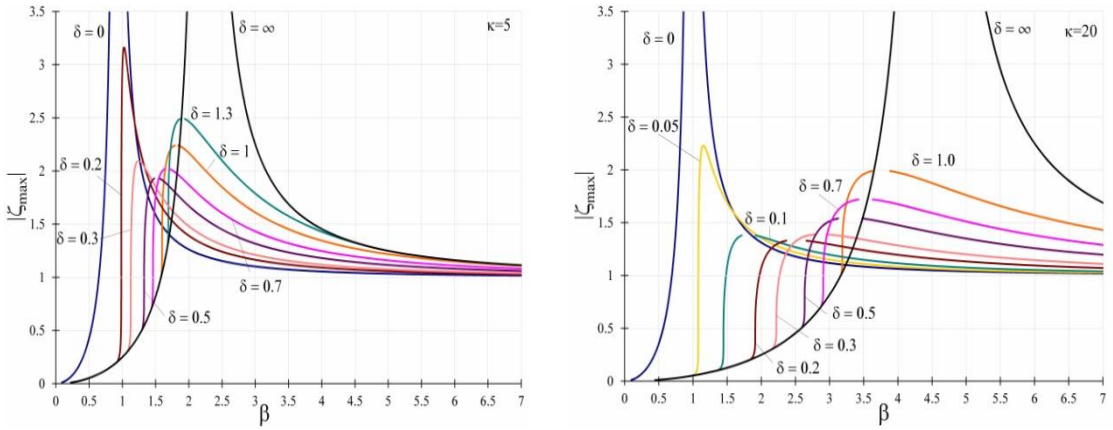

Fig. 8 Maximum deck displacement versus frequency ratio β (κ = 5, 20)

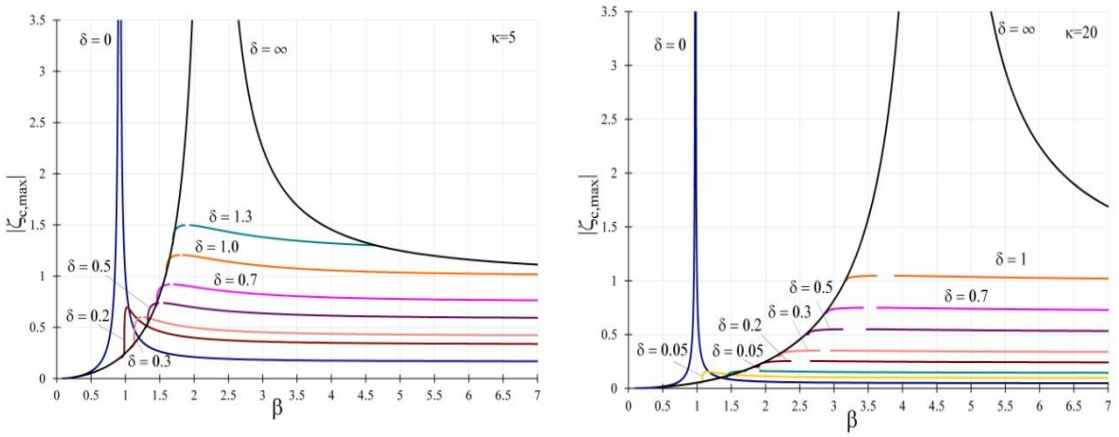

Fig. 9 Top column displacement versus frequency ratio β (κ = 5, 20)

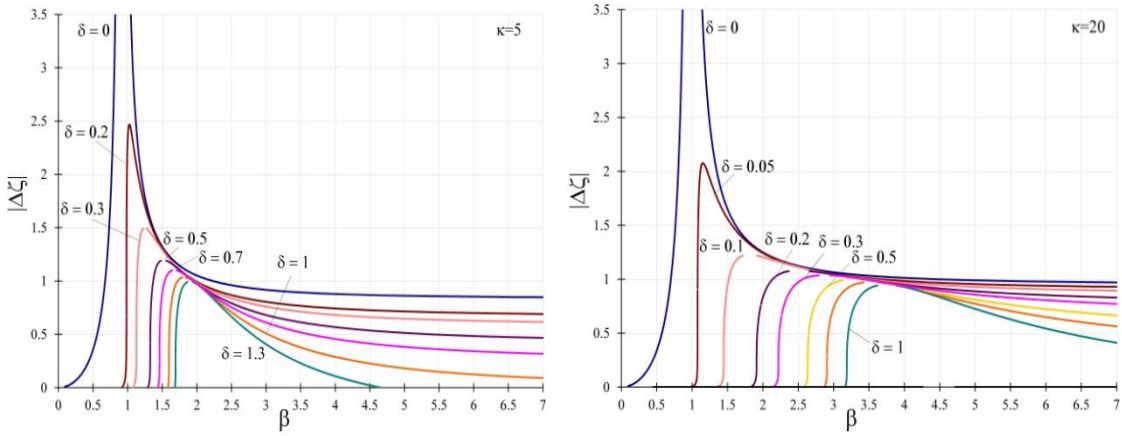

Fig. 10 Relative deck to pier displacement versus frequency ratio β (κ = 5, 20)

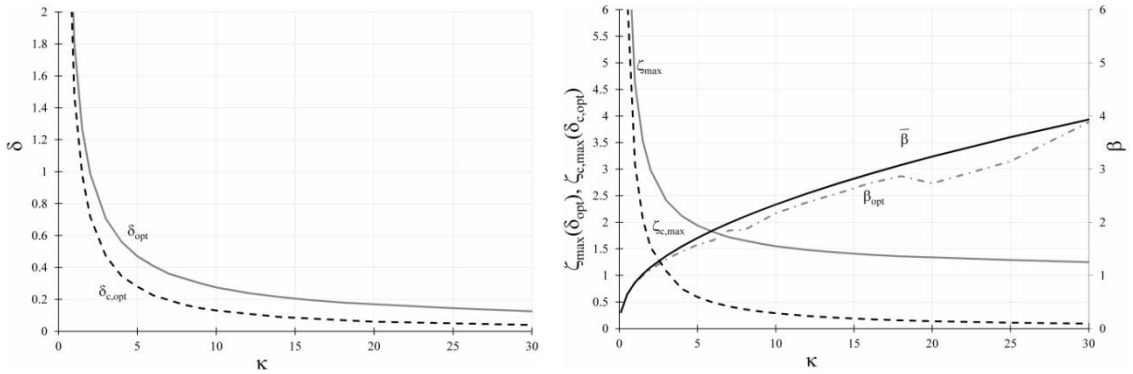

(a) (b)

Fig. 11 (a) *SI* optimal parameters for both deck and pier displacement and (b) deck optimal displacement, column optimal displacement, optimal frequency ratio and limit curves intersection point versus κ

3. Numerical validation of proposed design procedure

The design procedure proposed in the previous paragraphs has been verified through a numerical investigation performed on a typical isolated bridge having a target period $T_i = 2\cdot\pi/\omega = 2.5$ *s*. The equation of motion has been solved by implementing the Newton-Raphson integration method (Chopra 2011) in Matlab® environment (The MathWorks inc. 2010).

According to the Italian building code (NTC 2008), the design spectra (Fig. 12) with 5% of critical damping have been defined for the near collapse limit state of a bridge (functional class III) located in Grottaminarda, Italy (15.03° longitude, 41.06° latitude) on soil type B ($360 \le V_{s,30} \le 800$ m/s) with a nominal life of 50 years, corresponding to a return period of 1462 years. A set of seven unscaled spectrum matching accelerograms (Fig. 12, Table 2) was found in the European ground motion database using Rexel v3.4 beta (Iervolino *et al* 2010). The average spectrum has 10% lower and 30% upper tolerance in the period range 0.15-2 s.

In order to estimate the maximum expected ground displacement $x_{g,max}$ corresponding to the aforementioned spectra, it is necessary to compute the spectral displacement S_d in the long-period range up to 10 *s*. Several authors (Faccioli *et al.* 2004, Smerzini *et al.* 2013) and also the NTC suggest to assume the following relationship:

$$x_{g,\max} = 0.025 \cdot a_g \cdot S \cdot T_C \cdot T_D \tag{49}$$

where $a_g = 0.428$ *g* is the peak ground acceleration on bedrock, $S = 1.003$ is the soil amplification factor and $T_C = 0.547$ *s* is the control period corresponding to the beginning of the constant velocity branch of the design spectrum and $T_D = 3.310$ *s* is the corner period denoting the beginning of the maximum displacement plateau. Eq. 49 provides $x_{g,max} = 0.19$ *m* and this has been taken as reference for the *SI* case.

The response of the *VI* and *SI* bridge has been evaluated under seven ground motions characterized by different frequency content, to numerically determine the optimal values of the parameters ν_i and δ, and to compare them with those obtained from the analytical approach presented in the previous paragraph.

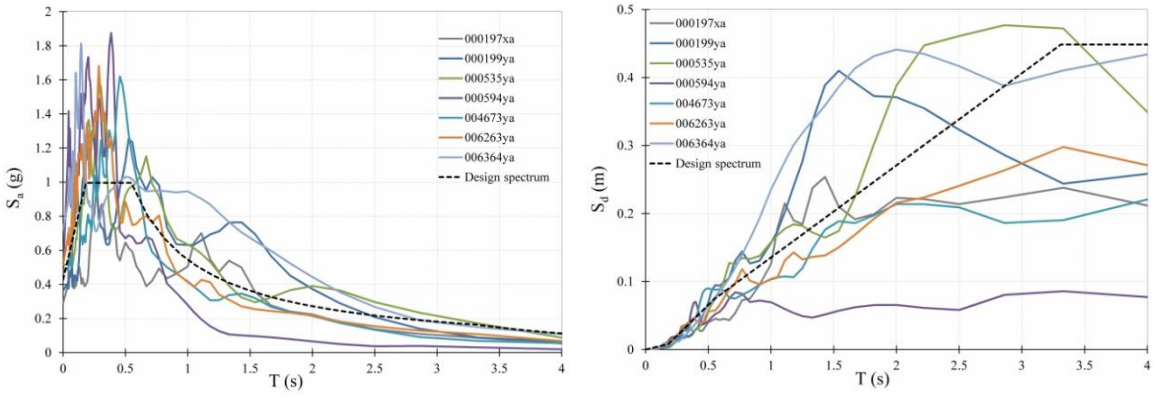

(a) (b)

Fig. 12 (a) Acceleration and (b) displacement design spectra (ν =5%) and selected ground motion spectra

Table 1 Selected spectrum-compatible accelerograms for site class B

Waveform ID	Earthquake ID	Station ID	Earthquake Name	M_w	Epicentral Distance [km]	PGA [m/s^2]	PGV [m/s]
4673	1635	ST2482	South Iceland	6.5	15	4.68	0.48
535	250	ST205	Erzincan	6.6	13	5.03	1.02
6263	1635	ST2484	South Iceland	6.5	7	6.14	0.50
199	93	ST67	Montenegro	6.9	16	3.68	0.52
197	93	ST63	Montenegro	6.9	24	2.88	0.47
6334	2142	ST2488	South Iceland (as)	6.4	11	7.07	0.97
594	286	ST60	Umbria Marche	6	11	5.14	0.32
mean:				6.54	13.86	4.94	0.61

Table 2 Bridge dynamic properties for rigid deck-to-pier connection

κ [-]	T_{fb} [s]	ω_{fb} [rad/s]	f_{fb} [hz]
5	1.12	5.59	0.89
20	0.56	11.17	1.78

Structural response is showed in the following both in terms of deck and top pier absolute displacement, and also of deck-pier relative displacement. The numerical investigation has been repeated for 2 different values of κ (5 and 20), which correspond to the following dynamic structural properties in case of rigid deck-to-pier connection (limit case $\nu_i \to \infty$ or $\delta \to \infty$ - Table 2):

Table 3 Bridge dynamic properties with $\nu_i = 0$ or $\delta = 0$

κ [-]	T_0 [s]	ω_0[rad/s]	f_0 [hz]
5	2.75	2.28	0.36
20	2.58	2.44	0.39

where $\omega_{fb} = \omega_i \sqrt{\kappa}$ and the corresponding normalized frequency β at resonance is $\sqrt{\kappa}$.

If no supplemental damping is provided (limit case $\nu_i = 0$ or $\delta = 0$), the dynamic properties of the system reduce to those in Table 3:

where the frequency $\omega_0 = \omega_i \sqrt{\frac{\kappa}{1+\kappa}}$ of the undamped structure corresponds to the normalized frequency ratio $\beta = \sqrt{\frac{\kappa}{1+\kappa}}$ at resonance.

A parametric investigation has been performed for each ground motion and for each value of κ, by assigning extremely different values to both ν_i (100 logarithmically spaced value between 10^{-3} and 10^5) and δ (100 logarithmically spaced value between 10^{-4} and 10): the pier and deck maximum displacements have been considered as result for each time history case and are plotted in what follows. The optimal parameter is the value corresponding to the minimum structural response in terms of pier or deck displacement, under each seismic excitation for a given κ.

The following figures summarize some relevant results of the numerical analyses performed on the case study for both control systems. In particular, the maximum normalized displacement is plotted versus the value of the parameter in a semi-logarithmic scale, so to make clear how different the response could be, ranging from one extreme to the other.

3.1 VI case

In the *VI* case, the structural model is defined as a two DOFs system (deck displacement *x* and pier displacement x_c - see § 2.2), where the only dynamic DOF is associated to the deck displacement. The equation of motion has been formulated as follows:

$$\mathbf{M} \cdot \ddot{\mathbf{x}} + \mathrm{C} \cdot \dot{\mathrm{x}} + \mathbf{K} \cdot \mathbf{x} = -\ddot{x}_g \mathbf{M} \cdot \mathbf{l}$$

where $\mathbf{x}^T = \begin{bmatrix} x & x_c \end{bmatrix}$, $\dot{\mathbf{x}}^T = \begin{bmatrix} \dot{x} & \dot{x}_c \end{bmatrix}$, $\ddot{\mathrm{x}}^T = \begin{bmatrix} \ddot{x} & \ddot{x}_c \end{bmatrix}$, $\mathbf{M} = \begin{bmatrix} m & 0 \\ 0 & 0 \end{bmatrix}$, $\mathrm{K} = \begin{bmatrix} k_i & -k_i \\ -k_i & k_c + k_i \end{bmatrix}$, $\mathrm{C} = \begin{bmatrix} c_i & -c_i \\ -c_i & c_i \end{bmatrix}$, $\mathrm{I} = \begin{bmatrix} 1 \\ 1 \end{bmatrix}$ and $\ddot{x}_g$ is the base acceleration.

In this case, the time step has been assumed equal to 0.01s while the parameters γ and β have been set to 1/2 and 1/4, respectively. Figs. 13 to 19 show the peak value of *x*, x_c and x-x_c under different applied earthquake records for the different values of ν_i. In the same figures, the vertical straight line indicates the optimal value determined from the proposed design procedure ($\nu_{i,opt}$ = 0.7171 for $\kappa = 5$, $\nu_{i,opt}$ = 0.7079 for $\kappa = 20$).

As expected, in all the analyzed cases, the response in terms of deck displacement shows a minimum value but this occurs for a value of ν_i almost always larger than the theoretically proposed one. With respect to the undamped case (ν_i=0), the deck response is strongly reduced. Main results are reported in Table 4:

Regarding top pier displacement, it is worth to note that an increase in the value ν_i is almost always responsible for a larger response of the column, due to the additional force transmitted by damping. However, it is clear from the above figures that top pier peak response slightly reduces for ν_i increasing between 0 and a value very close or slightly lower than $\nu_{i,opt}$. In other words, $\nu_{i,opt}$ represents a good compromise value which allows to optimize at the same time both the deck and top pier maximum displacement. Table 5 summarizes the numerical optimal values ν_i, always lower than $\nu_{i,opt}$:

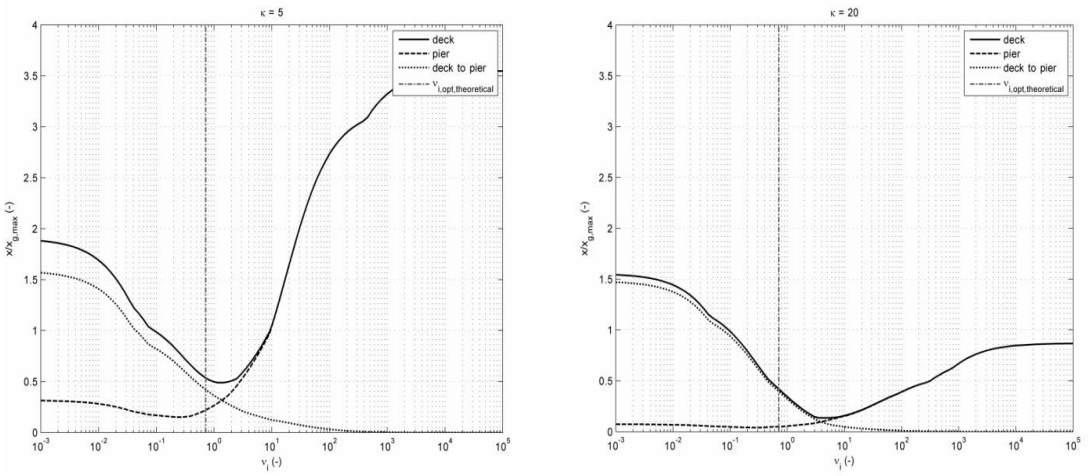

Fig. 13 *VI* case: numerical results for ground motion #197

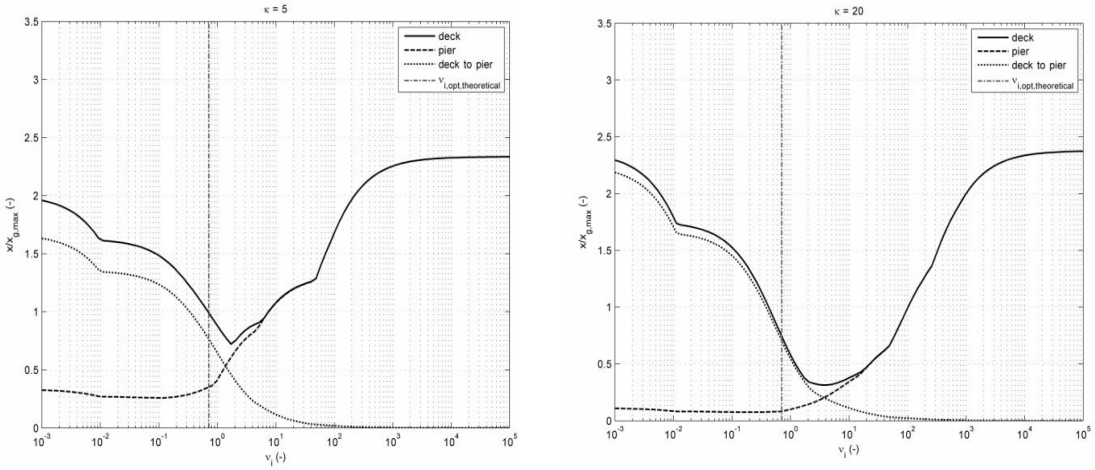

Fig. 14 *VI* case: numerical results for ground motion #199

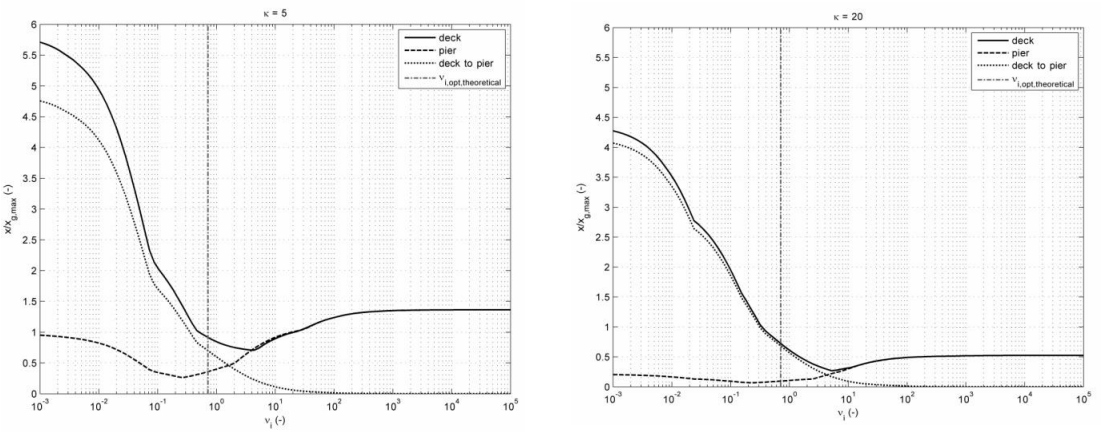

Fig. 15 *VI* case: numerical results for ground motion #535

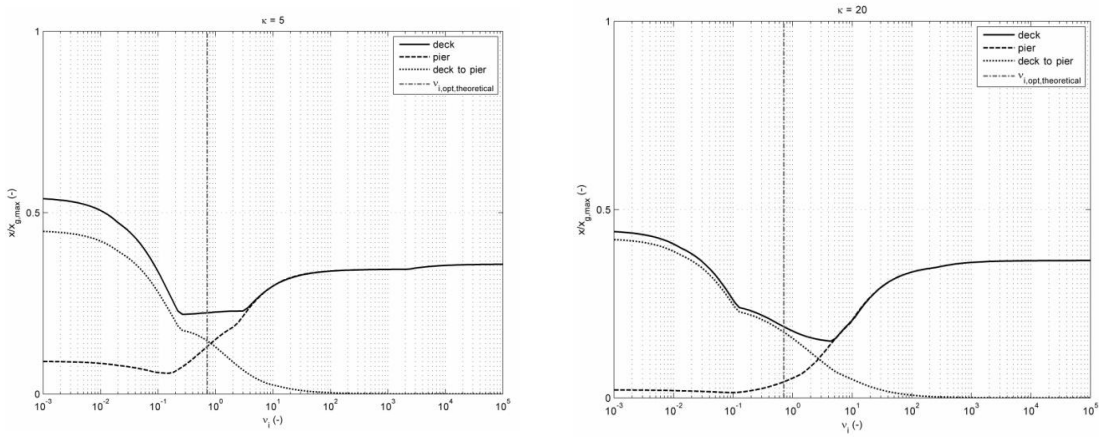

Fig. 16 *VI* case: numerical results for ground motion #594

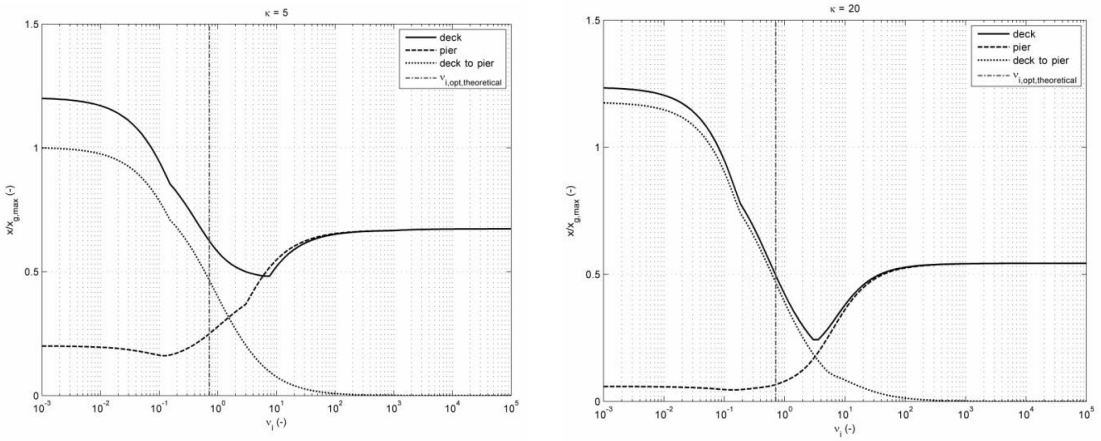

Fig. 17 *VI* case: numerical results for ground motion #4673

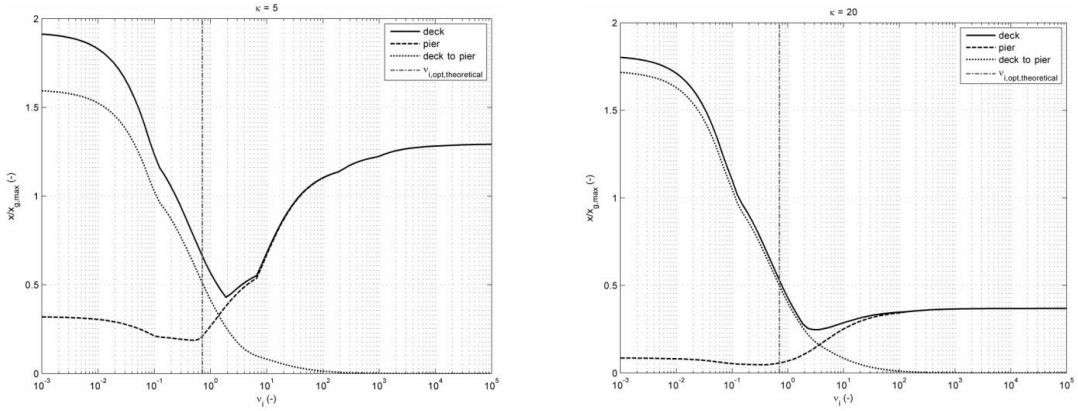

Fig. 18 *VI* case: numerical results for ground motion #6263

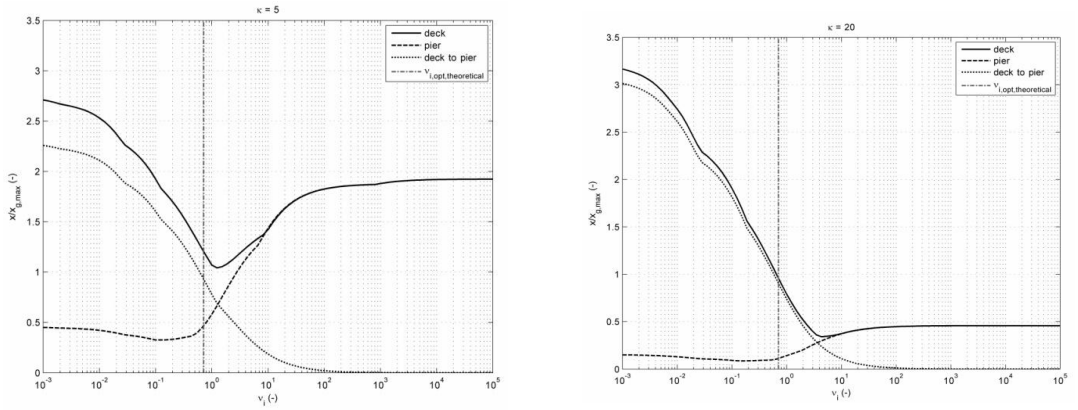

Fig. 19 *VI* case: numerical results for ground motion #6334

Table 4 Numerical optimum values of ν_i for the deck displacement

κ	#197	#199	#535	#594	#4673	#6263	#6334	$\nu_{i,opt}$
5	1.18	1.71	4.33	0.26	7.56	1.87	1.23	0.7171
20	4.33	3.59	5.21	4.32	2.98	3.51	4.32	0.7079

Table 5 Numerical optimum values of ν_i for the pier displacement

κ	#197	#199	#535	#594	#4673	#6263	#6334	$\nu_{i,opt}$
5	0.27	0.1	0.27	0.15	0.13	0.53	0.12	0.7171
20	0.32	0.22	0.22	0.09	0.15	0.35	0.15	0.7079

3.2 SI case

In the *SI* case, the structural model is defined as a bilinear single DOF system (see § 2.3). A time step of 0.0001s has been adopted to improve the accuracy of the integration with γ=1/2 and β=1/6. The damping ratio ν has been set equal to zero, due to the lack of supplemental viscous

damping.

Figs. 20 to 26 show the peak value of x, x_c and x-x_c under different applied earthquake records for the different values of δ. In the same figures, the vertical straight lines indicates the theoretically determined optimal δ for the deck (δ_{opt} = 0.47 for κ = 5, δ_{opt} = 0.17 for κ = 20) and for the column ($\delta_{c,opt}$ = 0.28 for κ = 5, $\delta_{c,opt}$ = 0.06 for κ = 20).

Differently from the *VI* case, the minimum of the deck response is not always between the two limit cases but sometimes reduces to the rigid deck-to-pier connection case, so implying the worst condition for the pier. For the value δ_{opt} the deck response is always reduced with respect to the undamped case (δ = 0). It must be noted that that the average of the actual numerical values in Table 6 is very close to the theoretically derived δ_{opt} :

Similarly to the *VI* case, due to the coupling effect with the deck, the pier displacement significantly increases with δ, except for a very low value of the ratio varying from 0 to a value lower than $\delta_{c,opt}$ (Table 7).

The outcome is that $\delta_{c,opt}$, instead of δ_{opt}, may be taken as design value able to strongly reduce the deck response while lightly affecting the pier response.

In a *SI* system, it has also been verified what is the effect of damping in the piers on the structural response: a value of ν=2% strongly reduces the response in case of elastic behaviour (δ = 0 or $\delta \to \infty$) while, in case of significant sliding in the isolation system, maximum displacements are mainly dependent on hysteretic dissipation (Fig. 27).

Table 6 Numerical optimum values of δ for the deck displacement

κ	#197	#199	#535	#594	#4673	#6263	#6334	δ_{opt}
5	0.13	0.67	0.46	0.17	0.32	0.36	1.24	0.47
20	0.12	0.22	0.22	0.03	0.15	0.32	0.46	0.17

Table 7 Numerical optimum values of δ for the pier displacement

κ	#197	#199	#535	#594	#4673	#6263	#6334	$\delta_{c,opt}$
5	0.032	0.006	0.13	0.011	0.02	0.057	0.05	0.28
20	0.005	0.057	0.027	0.002	0.013	0.013	0.017	0.06

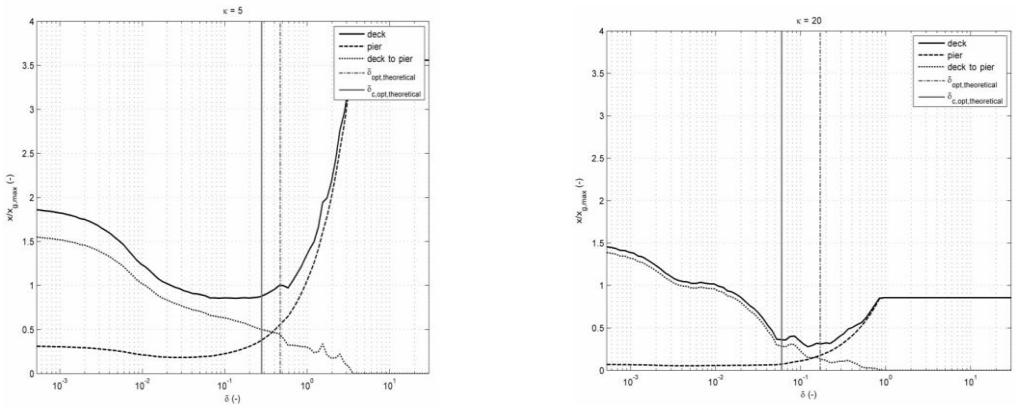

Fig. 20 *SI* case: numerical results for ground motion #197

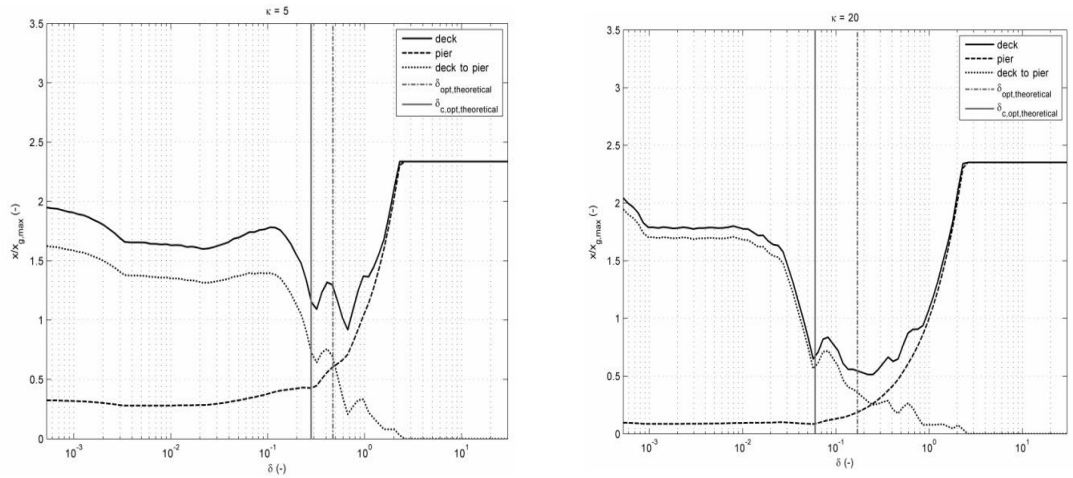

Fig. 21 *SI* case: numerical results for ground motion #199

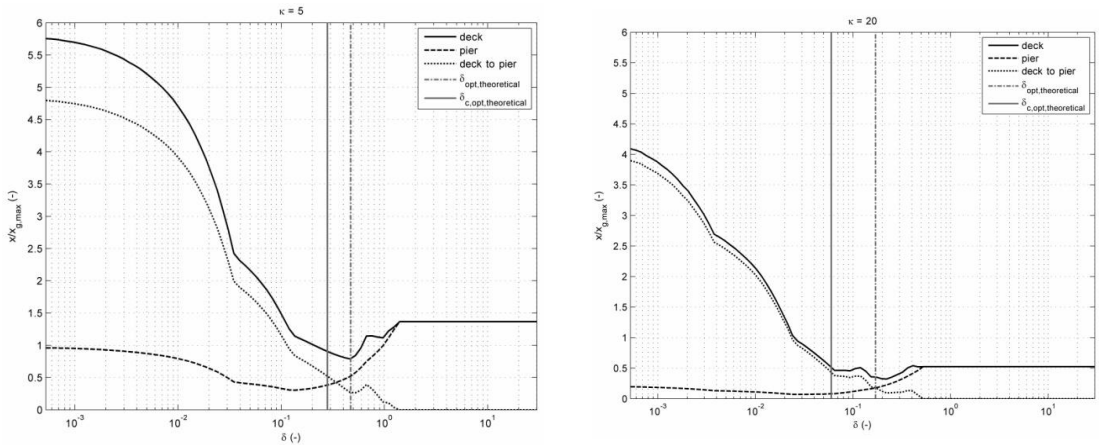

Fig. 22 *SI* case: numerical results for ground motion #535

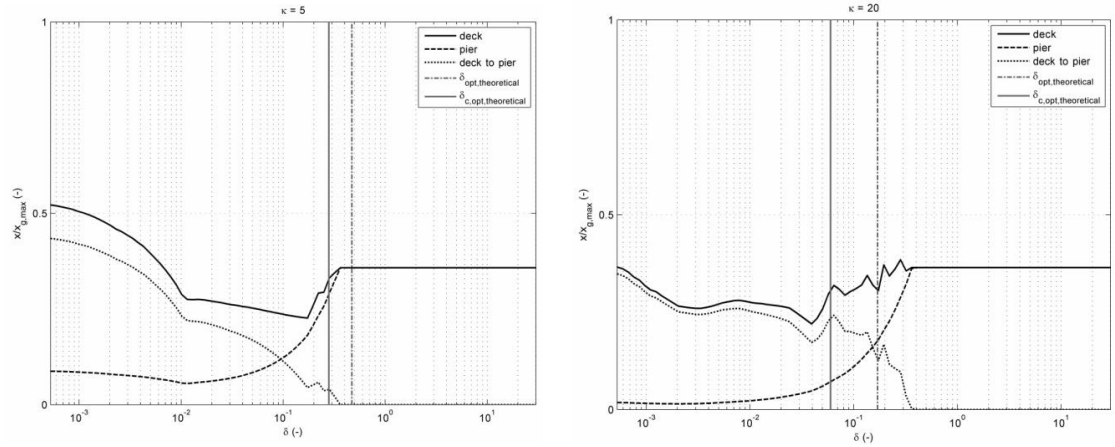

Fig. 23 *SI* case: numerical results for ground motion #594

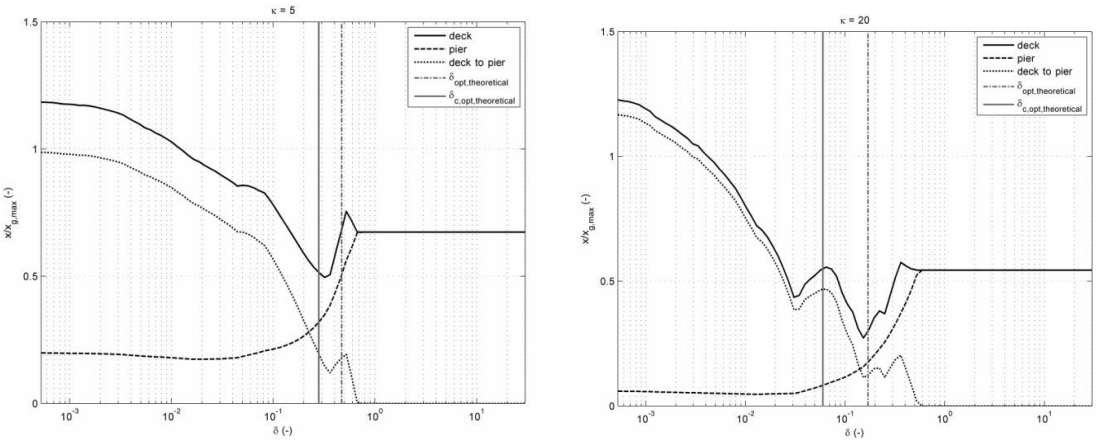

Fig. 24 *SI* case: numerical results for ground motion #4673

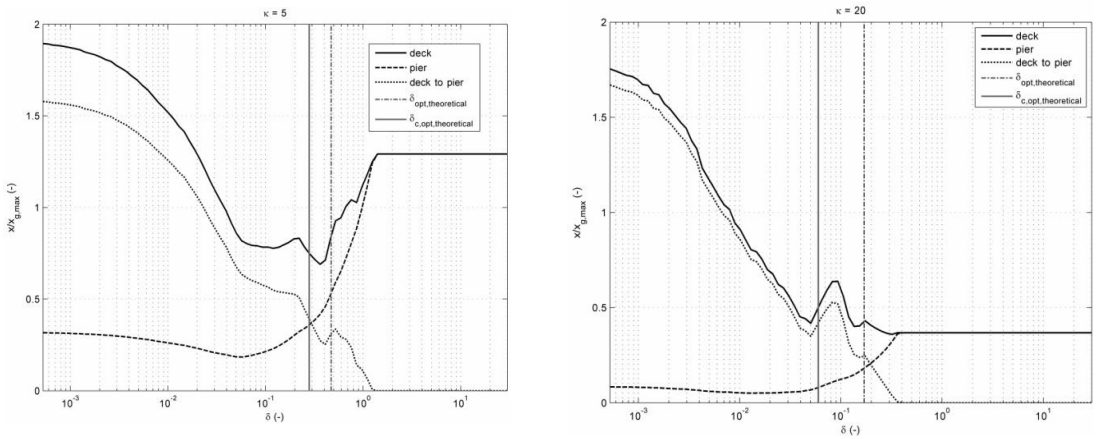

Fig. 25 *SI* case: numerical results for ground motion #6263

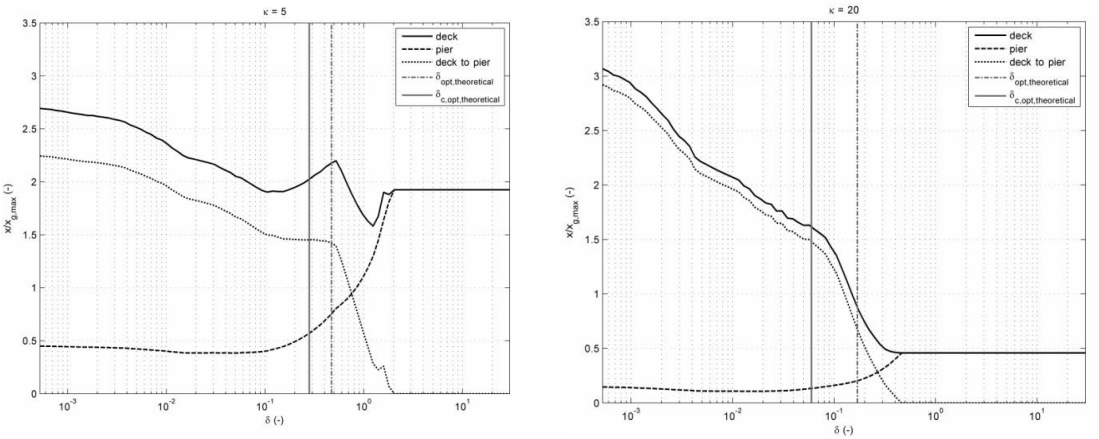

Fig. 26 *SI* case: numerical results for ground motion #6334

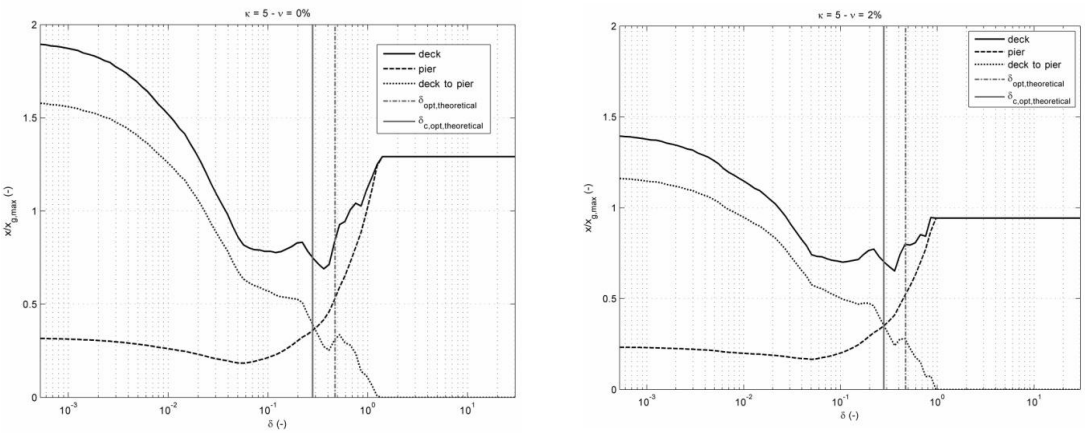

Fig. 27 Numerical results with additional viscous damping ν=2% for ground motion #6263

4. Design procedure

This paragraph summarizes the useful design method proposed by the authors. It has been developed taking into account the results of both theoretical treatment and numerical validation and is explained in the flowchart of Fig. 28. Given the fixed-base bridge properties, the stiffness of the isolation system k_i is defined to get a target period T_i. A starting value of the damping parameter is assumed equal to $\nu_{i,opt}$ or $\delta_{c,opt}$, from Fig. 6(a) or 11(a) respectively, since they were proved to be very close to the effective numerical optimum. Time history analysis are then performed under the code provided seismic action and the performance is checked a posteriori (i.e., average or maxima of results depending on the number of assumed accelerograms). If not satisfactory, a modification of the damping parameter can be made in order to get an improvement in the achievement of the desired target performance level (e.g. in terms of absolute minimum deck displacement). Some iterations could be needed to define the effective optimal values (ν_{opt} or δ_{opt}).

Near fault ground motion was not properly addressed in this work even if it is of great concern for structures with long natural periods (Jònsson e*t al.* 2010). Near fault effects are mainly characterized by low frequency pulses, short duration and higher horizontal accelerations with a significant component in the vertical direction too. Due to their natural period, base isolated structures are more vulnerable when subjected to near fault motion: for single pulse excitation, the maximum response mainly depends on the ratio of the impulse duration to the natural period of the structure while the influence of damping is expected to be negligible (Chopra 2011), so isoltators' displacement may significantly increase. In this case, at the stage of numerical validation, some accelerograms were selected with low epicentral distance (R<15 km) and no significant difference emerged from response.

Effects of different soil conditions and non-synchronous motion were neglected. The isolated bridge was designed as if subjected to a standard input motion, i.e., synchronous excitation and uniform soil condition. Its response under spatially varying ground motion can be evaluated by

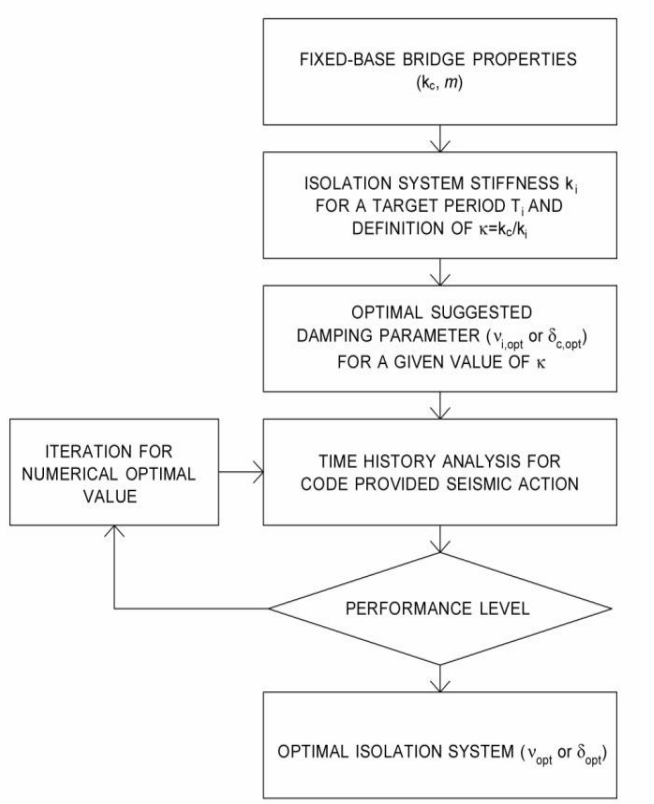

Fig. 28 Flowchart of the suggested design procedure

numerical simulations at the design stage. Design codes normally require consideration of ground motion spatial variability only for bridges several hundreds meters long, or in case of drastic variations of soil profiles. Eurocode 8 (CEN 2004) requires spatial variability to be considered in case of more than one ground type at the supports in case of continuous deck's length exceeding 200 m over soil type D (higher values are suggested in case of better soil conditions). In the formulation of the equation of motion with input spatial variability, the model must include the degrees of freedom at the supports so that kinematic vectors are splitted in *n*- unconstrained and *m*-support degrees of freedom. The *n*-vector x of the total displacements is the combination of a pseudo-static component x^s and a dynamic component x^d . The component x^s is computed from an *m*- vector u of prescribed support displacements while the term x^d is the effect of base accelerations. The spatial variation of the seismic action could be estimated using a simple approximative model based on pseudo-static effects of appropriate displacement sets imposed at the foundation of the supports, and then combined with the main inertial response. When a time-history analysis is performed, a sample acceleration motion, obtained by means of a vector of zero-mean random process having a power spectrum consistent with the elastic response spectrum, can be applied at each support, thus reflecting the probable spatial variability of the seismic action. Irrespective of bridge configuration, the displacement demand of most of the isolators increases inthe presence of spatial variability (Lupoi 2009). Especially in the case of non uniform soil

conditions underneath the bridge foundations (the source of the greater negative influence on the bridge response), specific studies are necessary and a safety factor approach cannot be pursued.

Pounding effects must be properly considered in a seismically isolated bridge, since lateral displacements are expected to increase significantly. Available clearances at deck movement joints and abutment back-walls must be checked in order to avoid collision, according to code requirements. A design criterion for the optimal isolation system was defined to obtain the minimum deck displacement, so implying minimum required clearances. It was proved that deck displacement is strongly reduced thanks to a value of damping very close to the optimal one, thus giving an optimal deck displacement not so different or sometimes lower than the fixed-base one. Taking benefits from damping, the question of pounding can be properly mitigated in seismically isolated bridges.

The procedure proposed by the authors was explained with reference to the Italian Code, where the collapse prevention limit state (SLC) has to be taken into account for the design of the isolation system: seismic action is defined for a 5% over 50 years probability of occurrence during the reference life V_R, whose value strongly affects the definition of the return period T_R (in this case about 1500 years). In the Eurocode 8 code non-collapse requirement must be fullfilled for bridge design at Ultimate limit state (ULS): an importance factor γ_I depending on the importance class of the bridge is provided to scale seismic action (for class II-average importance, T_R=475 years). In the US code, the maximum considered earthquake (MCE) must be taken into account in designing the isolation unit (ICC 2000), with a 2% probability of exceedance in 50 years.

In conclusion, the following recommendations are given: at the first-step of the design procedure, the suggested values of the reference parameters ($\nu_{i,opt}$ or $\delta_{c,opt}$) have to be assumed; then, after acceleration input motion has been defined according to code provisions, time history analysis need to be performed. Seismic input has to take into account, if necessary, near fault effects and ground motion spatial variability. Numerical results are then compared with the design performance level, that may concern minimum deck displacement or pier base shear. Even if initial suggested values were numerically validated for real ground motions, optimum definition is case-dependent and the achievement of the desired performance level may require some iterations due to randomness of earthquake. Actually, real strong motion properties (magnitude, duration, frequency content, etc.) may play an important role in the determination of the effective design optimal value.

5. Conclusions

In an isolated bridge deck, the increase in the horizontal period of vibration implies the need for supplemental damping in order to reduce the deck displacement. In this paper, a theoretical approach was suggested for determining the optimal value of the inherent viscous damping in case of viscoelastic isolators (*VI*) or the yielding force in case of sliding isolators (*SI*). The proposed method is based on the analytical determination of the response to a harmonic base motion, with the aim of obtaining the optimal values of the adimensionalized viscous damping parameter (ν_i) or yielding displacement (δ) able to minimize the structural response, for each value of the piers to isolators relative stiffness κ. The method can be applied to a single or multispan bridge, supported by two or more columns all having the same stiffness, isolated by means of elastomeric or sliding bearings.

The authors demonstrated that, given a certain target period of isolation T_i, for different values of the design parameters (ν_i or δ), the behavior would span between two extreme cases both corresponding to an undamped response with an unbounded resonance. The process of adding damping is not beneficial to any extent but just up to a certain level, depending on the objective of the optimization process. Within this field, the optimal values of ν_i and δ have been assumed as the ones corresponding to a minimum of the response curve in the overall frequency range, for the deck or the pier displacement. Design spectra are provided where theoretical optimal values are given as a function of κ.

In the second part of the paper, numerical analysis have been carried out to validate the proposed design method in case of two typical isolated bridges subjected to seven spectrum-compatible earthquake records for a near collapse limit state, according to the NTC. This was devoted to determine the change in the structural response produced by varying the parameters ν_i and δ.

The numerical analysis demonstrated that the value $\nu_{i,opt}$ minimizing the peak amplitude of the deck frequency response curve is usually of the same order of magnitude but slightly lower than that corresponding to the actual numerical optimum for the deck. This can be explained taking into account that the frequency content of a ground motion can vary significantly and does not correspond to a white noise exciting the overall range of frequencies of the system. Despite that, the theoretical value $\nu_{i,opt}$ is very close to the numerical optimum for the pier, being also able at the same time to significantly reduce the deck response.

As regard the *SI* case, it has been proved that δ_{opt} is in the average in good agreement with the numerical optimum values minimizing the deck response, the latter sometimes related to the rigid deck-pier connection behavior. On the other hand, the pier displacement increases with δ, a part for a small range of δ from 0 to a value lower than $\delta_{c,opt}$. In the *SI* case, numerical results are not only depending on the frequency content of the ground motion but also on the assumption regarding the definition of the maximum ground displacement $x_{g,max}$ that in the suggested analytical procedure represents the amplitude of the harmonic base motion and has been estimated by means of seismic hazard parameters. A part from the approximations and hypothesis of the method, $\delta_{c,opt}$ seems to be an acceptable value capable to strongly reduce the deck response without significantly affecting the pier displacement.

When designing an isolated bridge with elastomeric or sliding bearings, the optimal inherent viscous damping coefficient or the optimal sliding force, respectively, can be first adopted as $\nu_{i,opt}$ or $\delta_{c,opt}$. In this case the expected structural response is characterized by significantly reduced deck displacements with not affected or just lightly worsened pier response respect to the case $\nu_i = 0$ or $\delta = 0$. Both parameters can be assumed as a starting point in a case-dependent optimization process, therefore being necessary to perform iterative analysis for the code provided seismic action in order to check and find out the effective optimum value for the minimization of the desired response.

From numerical results it has also been observed that, for a given κ and ground motion, the absolute minimum deck displacement is obtained by means of viscous damping rather than hysteretic damping while for the minimum pier displacement there is no significant difference.

References

American Concrete Institute (ACI) Committee 318 (2011), "Building code requirement for structural concrete (ACI 318-11) and commentary", Farmington Hills, MI: American Concrete Institute

American Society of Civil Engineers/Structural Engineering Institute (ASCE/SEI) Committee 41 (2007), "Seismic Rehabilitation of Existing Structures", *ASCE 41-06* Reston, VI, 428.

ASTM Standard A706/A706M-13 (2013), "Standard specification for low-alloy steel deformed and plain bars for concrete reinforcement", ASTM International, West Conshohocken, PA

ASTM Standard A615/A615M-13 (2013), "Standard specification for deformed and plain carbon-steel bars for concrete reinforcement", ASTM International, West Conshohocken, PA

Bae, B. and Bayrak, O. (2008), "Plastic hinge length of reinforced concrete columns", *ACI Struct. J.*, **105**(3), 290-300

Baker, A. and Amarakone, A. (1965), "Inelastic hyperstatic frames analysis", *ACI Special Publication*, **12**, 85-142

Corley, W.G. (1966), "Rotational capacity of reinforced concrete beams", *Proceedings of the American Society of Civil Engineers*, **ST 5**, 121-146

Cosenza E., Manfredi, G. and Ramasco, R. (1993), "The use of damage functionals in earthquake engineering: a comparison between different models", *Earthq. Eng. Struct. Dyn.*, **22**, 855-868

Eleftheriadou, A.K. and Karabinis, A.I. (1999), "Seismic vulnerability assessment of buildings based on damage data after a near field earthquake", *Earthq. Struct.*, **3**(2), 117-140

Elwood, K.J. and Eberhard, M.O. (2009), "Effective stiffness of reinforced concrete columns", *ACI Struct. J.*, **106**(4), 476-484

Federal Emergency Management Agency (FEMA) (1997), "NEHRP Guidelines for the Seismic Rehabilitation of Buildings", FEMA-273, Federal Emergency Management Agency, Washington, DC, 435.

Federal Emergency Management Agency (FEMA) (2007), *Interim Testing Protocols for Determining the Seismic Performance Characteristics of Structural and Nonstructural Components*, FEMA-461, Federal Emergency Management Agency, Washington, DC, 138.

Ghannoum, W.M., and Moehle, J.P. (2012a), "Shake-table tests of a concrete frame sustaining column axial failures", *ACI Struct. J.*, **109**(3), 393-402.

Ghannoum, W.M and Moehle, J.P. (2012b), "Dynamic collapse analysis of a concrete frame sustaining column axial failures", *ACI Struct. J.*, **109**(3), 403-412.

Sezen, H. and Moehle, J.P. (2006), "Seismic tests of concrete columns with light transverse reinforcement", *ACI Struct. J.*, **103**(6), 842-849

Ghannoum, W.M., Saouma, V., Haussmann, G., Polkinghorne, K., Eck, M. and Kang, D.H. (2012), "Experimental investigations of loading rate effects in reinforced concrete columns", *J. Struct. Eng.*, **138**(8), 1032-1041

Gérin, M. and Adebar, P. (2009), "Simple rational model for reinforced concrete subjected to seismic shear", *J. Struct. Eng.*, **135**(7), 753-761).

IAAE 1996 - IAEE (1996), Regulations for Seismic Design. International Association for Earthquake Engineering, a world list.

Kim, Y., Quinn, K.T., Satrom, C.N., Ghannoum, W.M. and Jirsa, J.O. (2011), "Shear strengthening RC T-beams using CFRP laminates and anchors", *ACI Special Publication*, SP**275**-36, 1-18.

Leborgne, M.R. (2012), "Modeling the post shear failure behavior of Reinforced concrete columns", Ph.D. dissertation, The University of Texas at Austin, Austin, TX.

Lehman, D., Moehle, J., Mahin, S., Calderone, A. and Henry, L. (2004), "Experimental evaluation of the seismic performance of reinforced concrete bridge columns", *J. Struct. Eng.*, **130**(6), 869-879.

Lynn, A.K. (2001), "Seismic evaluation of existing reinforced concrete building columns", Ph.D. dissertation, University of California at Berkeley, Berkeley, CA.

Mathworks (2014), "Matlab Image Processing Toolbox", http://www.mathworks.com/products/image/

Macchi, G., Pinto, P.E. and Sanpaolesi, L. (1996), "Ductility requirements for reinforcement under Eurocodes", *Struct. Eng. Int.*, **6**(4), 249-254.

Mendis, P. (2001), "Plastic hinge lengths of normal and high-strength concrete in flexure", *Adv. Struct. Eng.*, **4**(4), 189-195.

National Instruments, 2014, "NI Vision Development Toolbox", http://www.ni.com/labview/vision/
Park, Y.J and Ang, A.H.S. (1985), "Mechanical seismic damage model for reinforced concrete", *ASCE*, **111**(4), 722-757
Paulay, T. and Priestley, M.J.N. (1992), *Seismic Design of Reinforced Concrete and Masonry Buildings*, John Wiley and Sons, Canada
Priestley, M.J.N., Seible, F. and Calvi, G.M. (1996), *Seismic Design and Retrofit of Bridges*, John Wiley and Sons, Inc., New York
Priestley, M.J.N. (2003), "Myths and fallacies in earthquake engineering, revisited" (In the Ninth Mallet Milne Lecture), Rose School, Pavia, Italy., 9-31
Saatcioglu M. and Ozcebe, G. (1989), "Response of reinforced concrete columns to simulated seismic loading", *ACI Struct. J.*, **86**(1), 3-12
Verderame, G.M., Fabbrocino, G. and Manfredi, G. (2008), "Seismic response of RC columns with smooth reinforcement. Part II: Cyclic tests", *Eng. Struct.*, **30**(9), 2289-2300

SA